Tagging secondary vertices produced by beauty decay and studies about the possibilities to detect charm in the forward region at the ZEUS experiment at HERA

Silvia Miglioranzi
University College of London / Argonne National Laboratories

June 20, 2003

Abstract

An algorithm designed to detect secondary vertices produced by mesons containing beauty quark is described. The information provided by the new Silicon Micro Vertex Detector is included. Monte Carlo samples were used to simulate the photoproduction of $b\bar{b}$ events. A preliminary comparison of Monte Carlo with 2002 data is also presented. Moreover a preliminar study concerning the possibility to detect charm (D^*) in the forward region (up to $\eta = 2$) is shown.

Contents

List of Figures

1 Introduction

The Hadron Electron Ring Anlage (HERA) is the only lepton-nucleon collider in the world [1]. It consists in two separeted accelerators, for the electron and proton beam respectively: it is designed to accelerate 27.5 GeV positrons and protons up to 920 GeV producing collisions of 318 GeV center of mass energy. It was built 10-30 m underground and in a ring with a diameter of 6.34 km. The tunnel where it is situated is under the Volkspark of Hamburg.
ZEUS is a multipurpose detector designed to study the lepton proton collisions. The detector has an angular coverage of almost 4π (if are not considered the small regions around the beam pipe). In Fig. 1 it is shown the transverse section of the detector: near the interaction region are placed the central tracking detectors.

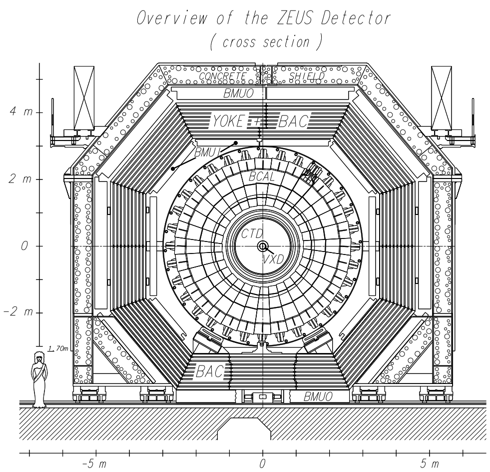

Figure 1: Transverse view of the ZEUS detector.

The CTD, placed in a solenoidal magnetic field (B=1.43 T), is the main tracking device; recently in 2001 it has been installed a Silicon Micro Vertex Detector (MVD) [2] and a Straw Tube Tracker (STT) [3] in the forward region allowing a signifincantly improvement of the tracking capabilities and improving the acceptance for high-mass and high-Q^2 events.
The MVD allows to reconstruct and tag heavy flavours particles by tracks displaced from the primary interaction vertex and by secondary vertex reconstruction. Outside the solenoid region is placed an Uranium-scintillator Calorimeter (UCAL) and even more external, the muon chambers (FMUON, BMUON, RMUO) and, in the leptonic beam direction a luminosity monitor (LUMI).

2 Track and vertex reconstruction

The program used in ZEUS for the tracks and primary and secondary vertices reconstruction inside the detector is called VCTRAK [4]. Every track reconstructed must contain CTD hits even if information from the other tracking detectors (MVD,SRTD,RTD,FTD1) could be taken into account.

For this analysis I have used a new version of VCTRAK which use the information coming from the new MVD. In HERA II this ZEUS component is essential to study the decay of particles containing heavy quarks. If we consider that the decay in the transverse plane of a generic particle of mass m, mean decay length $c\tau$ and transverse momentum P_t is approximately:

$$P_t \cdot \frac{ct}{m} \tag{1}$$

hadrons with a momentum of few GeV and mean lifetime of the order of 10^{-12} can be clearly distinguished from the primary vertex if $c\tau$ is sufficiently high (of the order of $10^2 \mu m$). In order to study the decay of b-mesons particle identification and secondary vertex reconstruction is needed.
Tracks and vertices reconstruction can be summarized in three steps:

- pattern recognition
- track fit
- vertex identification

2.1 Pattern recognition

Since the magnetic field is almost axial in the interaction region, the particle trajectory is considered, in first approximation, a cylindrical helix along the z axis. In the pattern recognition (PR) in order to parametrise the helix in 3 dimensions the following parameters are considered:

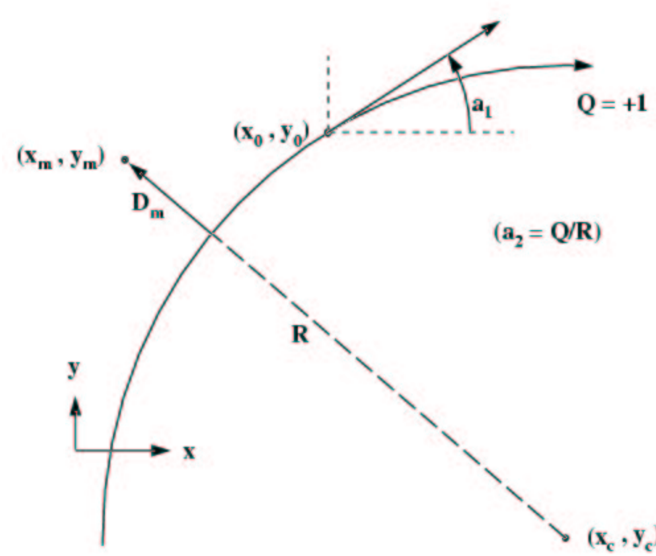

Figure 2: Helix parametrization in the Pattern Recognition step. The reference point to the trajectory is (x_0, y_0);(a_1,a_2) are the fit parameters in the XY plane.

- two parameters in the XY plane:(a_1,a_2) as shown in Fig. 2

- two parameters in the plane sZ:(p_1,p_2), where s is the path along the curve. Considering an s path in 2D on the circunference, $Z = p_1 + sp_2$, where $p_1 = z$ ad (x_0, y_0) e $p_2 = cot(\theta)$.

The reference point for the trajectory corresponds to the most external hit in (x_0, y_0) [6].
This track parametrization method is faster then the one used in the fit step which uses 5 parameters, a good feature if this algorithm run also at the third level trigger (TLT). The pattern recognition starts at the external point of the tracking system towards the internal region, therefore in the CTD this process begins in the most external axial superlayer. When a track segment is found, only the ones made by 4 hits or more are kept. The sense CTD wires are positioned along a slightly curved path in order to solve the left-right ambiguity.

2.2 Track fit

In the interaction region the magnetic field generated by the solenoid is approximately parallel to the CTD axis so a parametrization like the one shown in Fig. 3 can be used.

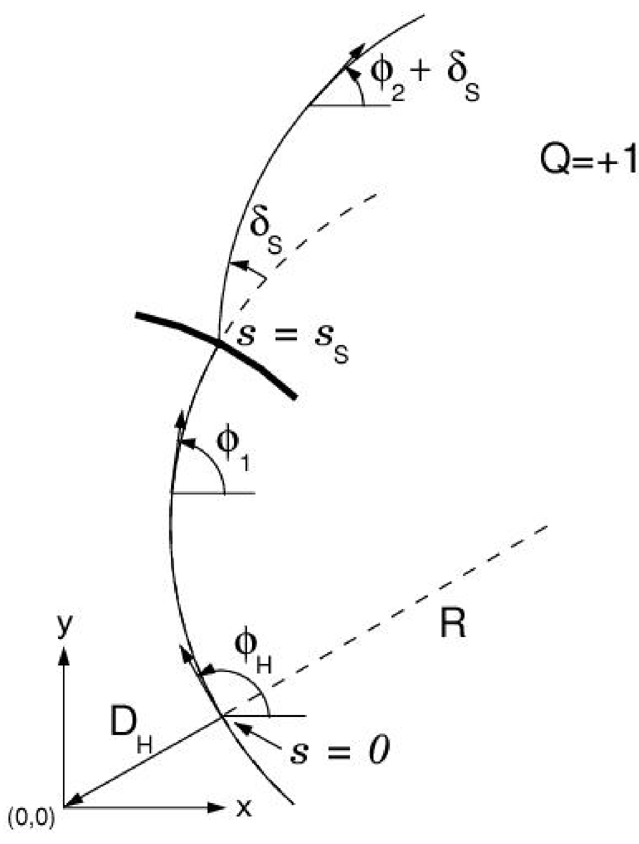

Figure 3: VCTRAK helix parameterization in the track fit process.

This helix parametrization uses 5 parameters and an arbitrary reference point (X_{ref}, Y_{ref}) which is taken at (0,0). The parameters are:

1. ϕ_H, the azimuthal angle of the helix tangent in the closest approach point to the straight line x = y = 0;
2. Q/R, where Q is the track charge and R the local radius of curvature;
3. QD_H, the distance of closest approach to the straight line x = y = 0;
4. Z_H, the z coordinate of the track in the closest approach point to the line x = y = 0;
5. cotθ_H, where θ_H is the polar angle of the track.

The point of closest approach to the reference point could be written as:

$$\begin{cases} X_H = X_{ref} + QD_H sin\phi_H \\ Y_H = Y_{ref} - QD_H cos\phi_H \\ Z_H \end{cases} \tag{2}$$

If we consider that the path along the curvature of a generic trajectory in the XY plane is:

$$(s(\phi) = -QR(\phi - \phi_H) \tag{3}$$

we can parametrize the coordinates of a generic point of the helix like:

$$\begin{cases} X = X_H + QR(-sin\phi + sin\phi_H) \\ Y = Y_H + QR(+cos\phi - cos\phi_H) \\ Z = Z_H + s(\phi)cot\phi \end{cases} \tag{4}$$

the three components of the momentum will be:

$$(p_x, p_y, p_z) = (p\cos\phi sin\theta, p\sin\theta\sin\phi, p\cos\theta) \tag{5}$$

2.3 Vertex finding

The tracks parameters obtained in the fit step are the input information to the vertex finding process. The main goal of the pattern recognition phase is to find the primary vertex. Each vertex is defined by the track trajectories which are "forced" to its position (detail about this procedure can be found [5]). It is possible to choose the following modes:

"primary vertex only" mode which does not perform the secondary vertex finding

"multi vertex" mode which finds primary vertices which are compatible with the existence of secondary vertices. The execution time is longer (it is in fact used "Off-line") but there are evident advantages:

- many events in which the primary vetices were not found in mode A) now are defined in mode B) (usually they are events with a low primary tracks multiplicity and many secondary tracks).

- the primary vertex finding is "clearer" because the tracks which contaminated the primary vertex now are associated to a secondary one.

2.4 MVD information included in VCTRACK

At the end of last summer (2002) was ready a new version of VCTRAK which includes the information from the Micro Vertex Detector; there are many advantages with respect to the old one exploiting only the CTD information:

- track finding efficiency: since the MVD is included in the initial pattern recognition phase, a 3% globally increment in the efficiency is obtained.

- improvement in the trajectory resolution.

- vertex finding: the primary vertex resolution appears improved together with the efficiency in the secondary vertices finding. In other words, those tracks formerly wrongly associated to the primary vertex, now can be properly identified. The effective improvement in the interaction vertex resolution using the MVD, can be seen in Fig. 4 where the resolutions on the primary vertex coordinates using a beauty photoproduction Monte Carlo sample are plotted. In the left column (a), c) and e)) is shown the vertex resolution using only the CTD information, while in the right one (b), d) and f)) we can observe the same distribution taking into account also the MVD hits.

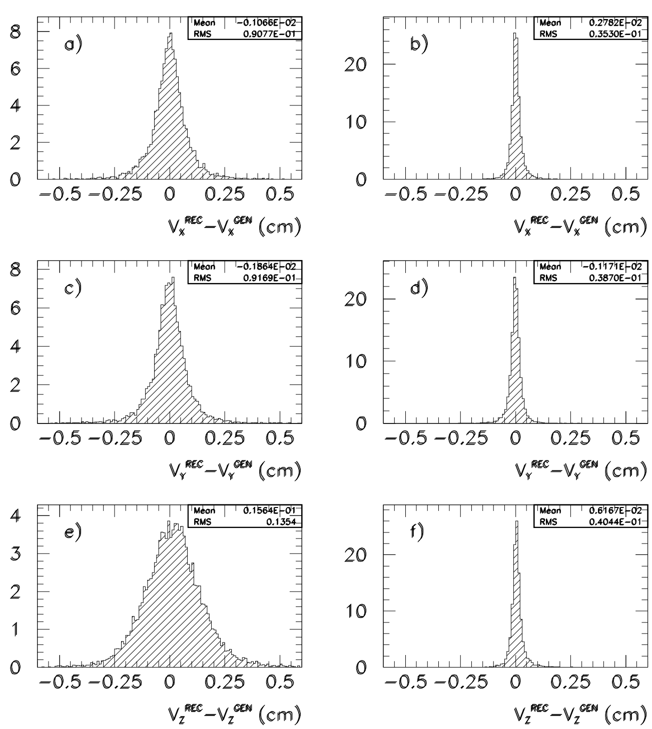

Figure 4: Primary vertex coordinates distribution in a Monte Carlo sample with beauty photoproduction; in the left column only CTD information are used, in the right column the MVD hits are also taken into account.

3 Secondary vertices and jet tag

Our goal was to obtain an algorithm to find secondary vertices in photoproduction events with 2 jets with high transverse momentum in the final state. This algorithm could be associated to the selection of muons with high Pt in order to have a double tag of beauty quark.
The purpose of this kind of study is to calculate a variable sensitive to the mean lifetime of the hadrons and show, studying the distribution of this variable, to discriminate the beauty signal from the light flavour signal. We used Monte Carlo samples to simulate events with the beauty, charm and light flavour production. We generate events with PYTHIA [] using for the charm and beauty mass the values m_c=1.35 GeV and m_b=4.5 GeV respectively.
The energy of the electron and the incident proton was fixed at E_e=27.5 and E_p = 920 GeV respectively. In order to optimize the generation of events with high transverse momentum, we required at least two jets with transverse energy E_t^{jet} ≥5 GeV and pseudorapidity $\eta^{jet} \leq 3$ GeV for the beauty and charm samples, while the requirements for the light flavour samples were E_t ≥5.25 GeV and η ≤3 GeV. For the background sample, we required a minimum transverse momentum , at partonic level, equal to 4 GeV/c. All these requirements produced a "reduction factor" R that has to take into account when the luminosity is calculated. If N is the number of generated events and σ the total cross section for the considered subprocesses, the luminosity is:

$$L = \frac{N}{R} \times \sigma. \tag{6}$$

The generated events were processed trough the chain of ZEUS programs which simulate the geometry and the detector (MOZART [7]) and which reconstruct the event (ZEPHYR [8]). In this preliminary phase the trigger simulation is not yet available. The MOZART simulation, moreover, contains some approximations, e.g. the interaction was simulated at a fixed primary vertex:

$$\begin{cases} x_V = 1.75 & cm \\ y_V = 0 & cm \\ z_V = 0 & cm \end{cases} \tag{7}$$

In the new version, now available, the primary vertex is randomized according to the distribution obtained from real data. For this reason we are re-processing our MC samples with the new version of Mozart. In this study we used also information about jets which are reconstructed adopting a cluster algorithm called "k_t" algorithm which groups couple of particles close in the phase space and merging them in order to create new "pseudoparticles" that are considered in the further iteration [9]. In order to improve the hadronic final state reconstruction it is usefull to combine the calorimetric information with the tracking information; this kind of hadronic reconstruction is called ZEUS EFO (Energy Flow Object). The hadronic total energy is given by summing all the particles contributions (charged and neutral) which can be efficiently detected through the calorimeter; the possibility to use for the charged tracks also the information coming from the tracking devices, often improves the precision especially at low energies.

3.1 Reference Sample

In order to define a photoproduction reference sample, we applied some requirements like the ones applied for the real data selection:

- we removed the events in which an electron was reconstructed with a probability $P(e) \geq 0.9$ [10] and energy $E'_e \geq 5$ GeV and we consider:

$$y_{el} = 1 - \frac{E'_e}{2E_e}(1 - \cos\theta'_e) \leq 0.9 \tag{8}$$

  where E_e=27.5 GeV is the energy of the incoming beam and θ'_e is the polar angle of the electron reconstructed in the final state.

- we required:

$$0.2 \leq y_{JB} \leq 0.8 \tag{9}$$

  where y_{JB} is an inelasticity estimator of the event; it is defined as:

$$y_{JB} = \frac{E - P_z}{2E_e}. \tag{10}$$

In (10) $E - P_z$ is the difference between the total energy and the longitudinal momentum of the system reconstructed in the final state. At HERA this quantity has a fixed value. Using the 4-momenta of the electron and proton incident beam we have:

$$E - P_z = 2E_e \simeq 55 \quad GeV \tag{11}$$

In DIS interactions where the scattered electron is considered in the $E - P_z$ calculation, we expect a $E - P_z$ peak near the nominal value (11). In photoproduction events, in which the electron in the final state escape inside the beam pipe, we obtain lower values for the reconstructed quantity $E - P_z$. Therefore requiring $y_{JB} < 0.8$ we removed residual DIS events with an electron not identified in the calorimeter. The final samples are finally selected requiring at least 2 reconstructed jets in the final state, with transverse momenta $P^{jet}_{T1,2} > 8, 7$ GeV respectively and pseudorapidity $\mid \eta^{jet} \mid < 2.5$.

3.2 Track selection for secondary vertices reconstruction

The track reconstruction program (VCTRAK) yields all the secondary vertices of the event, determined through an iterative procedure which allows to add or subtract tracks form the calculation in an independent way, without recomputing all the parameters from the beginning. For this reason we could modify the original routine which calculate the primary vertices transforming it in an algorithm to calculate the secondaries, after eliminating from the fit the “beam constraint” which forced the search of the beam interaction point in a specific transverse region. Using VCTRAK we developed an independent program which repeats the tracks fit to determine both primary and secondary vertices. In order to detect secondary vertices produced by the decay of the B mesons, we used only tracks with the following requirements:

- $p_T > p_T^{min}(0.5$ GeV/c)
- $\#SuperLayerCTD > 3$
- Total number of hits inside MVD> 4
- $\chi^2_{elica} < 100$

3.3 Tracks-jet association and jet-tagging with a secondary vertex

Every track which pass the above mentioned cut was associated to the closest jet in the (η, ϕ) plane according to the distance R defined as:

$$R = \sqrt{(\eta_{traccia} - \eta_{jet_{1,2}})^2 - (\phi_{traccia} - \phi_{jet_{1,2}})^2} \tag{12}$$

and requiring $R < 1$. In fig. 5 the distribution of this variable and the applied cut are shown. Those tracks which

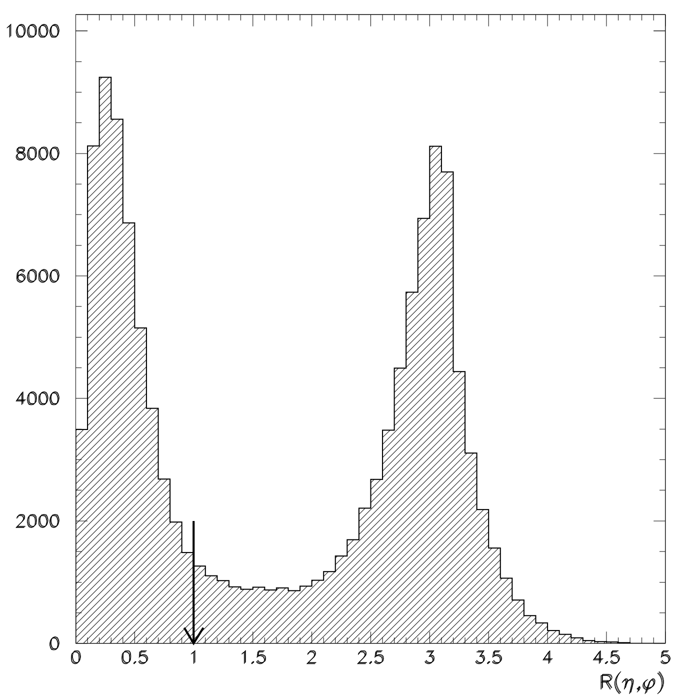

Figure 5: R variable distribution; this quantity is used to define the helix-jet association. We required $R < 1$.

survive to the selection and that are associated to the same jet are then put in input to the algorithm which find the common vertex.
If then the algorithm successfully find a vertex, the fit procedure will provide in output the three vertex coordinates, the covariance matrix and the χ^2. In fig. 6 the secondary vertex resolution is shown compared with the reconstructed vertex with the Monte Carlo vertex, for the photoproduction beauty sample.

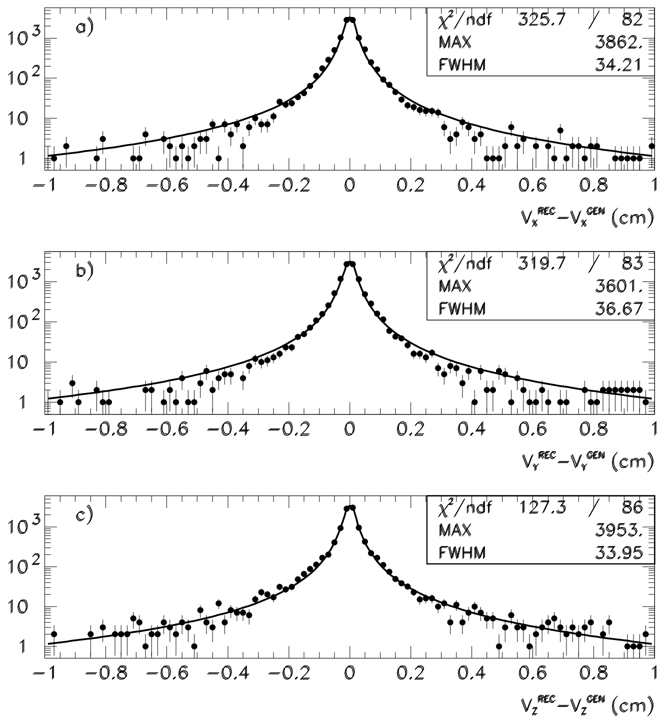

Figure 6: Resolution of the secondary vertices coordinates in a $b\bar{b}$ direct photoproduciton Monte Carlo sample. The distributions are fitted with a Breit-Wigner curve.

The distribution was calculated considering jets with a secondary vertex tagging and associating those jets to the primary hadron using an angular distance criterium. The distributions show non-gaussian tales. Using a fit with the Breit-Wigner function, we can have quite good agreement with the data but this function itself it is not enough. The typical resolutions are around 35 μm FWHM, which are consistent with the expectation.

3.4 Decay distance

Once the secondary vertices and the associated jets were found, we calculated the transverse decay distance like:

$$L_{xy} = \mid \vec{S} - \vec{P} \mid ((\vec{S} - \vec{P}) \cdot \hat{j}) \tag{13}$$

where $\vec{P}$ and $\vec{S}$ are the position vectors of the primary and secondary vertex respectively and $\hat{j}$ is the versor along the jet axis.

We considered also the decay distance in 2dimensions, in the transverse plane L_{xy}, defined in a similar way using the position vectors in the transverse plane. The decay length defined above has a specific sign which is determined from the position of the secondary vertex with respect to the primary vertex and form the jet direction. If the secondary vertex is in the same side of the primary vertex and of the jet, this length is positive, otherwise it is considered negative.
The decay length distribution is shown in fig. 7 for the different samples we used (a) beauty, b) charm and c) light flavour).

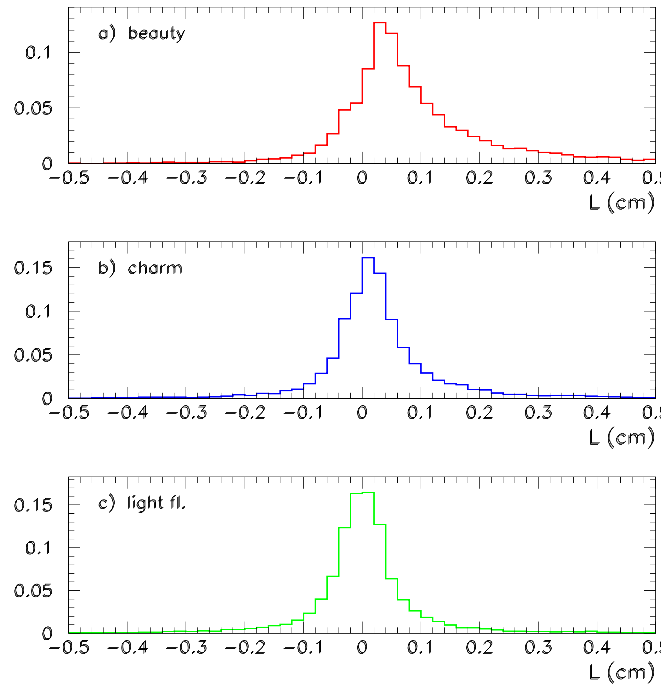

Figure 7: Decay distance distribution in a) beauty b) charm c) light flavour Monte Carlo samples.

The direct and resolved Monte Carlo for the beauty , charm and light flavour production were combined renolmalizing them to the same luminosity (using the predicted Monte Carlo cross sections).
The negative values of the variable L that we can observe in the signal plots (beauty) are due to those events in which the heavy quarks decay near the interaction region and the finite resolution of the MVD gives a wrong reconstruction of the secondary vertex behind the primary. In these plots a secondary vertex is reconstructed using at least two tracks. We can observe, like we expect, that the L distribution is asymmetric towards positive values for the beauty sample, while it is almost symmetric for the background sample (light flavour).
The significance of the distance L is measured in terms of standard deviations, considering the ratio L/σ, where σ represents the error on L and both the contributions of the primary and the secondary vertex (covariance matrix elements) are considered. We should take into the account the fact that our study contains an approximation:

the tracks which are associated to a secondary vertex are not subtracted from the primary vertex; in other words, we always use the primary vertex obtained considering all the tracks (a more sophisticated procedure could impose to recalculate the jets using the new primary vertex). In fig. 8 the significance distribution $\mid L \mid / \sigma$ is plotted.

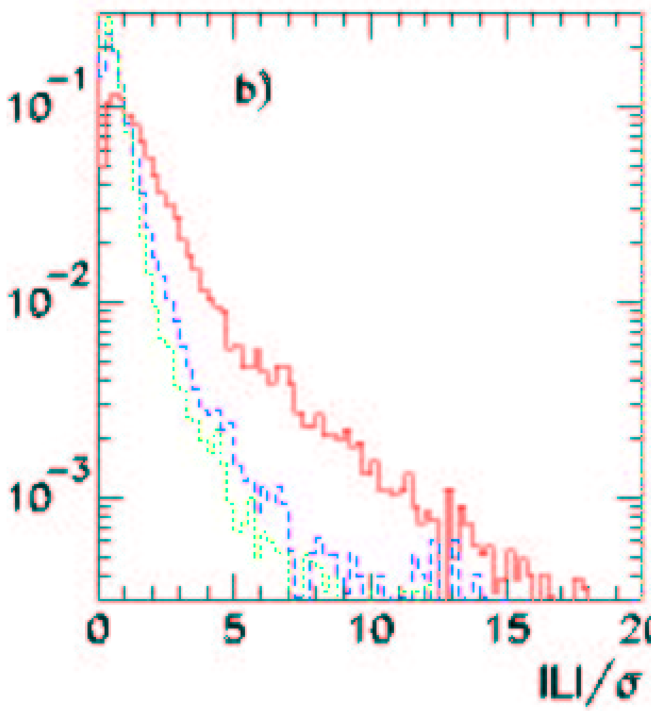

Figure 8: $\mid L \mid / \sigma$ distribution for beauty (red), charm(blue), and (green) light flavours.

These distributions have a different shape for the signal (beauty) if compared to the background due to the charm and the light flavours. A cut on $\mid L \mid / \sigma = 1$ can be used to improve the signal/background ratio.
In fig. 9 the fraction of signal and background reference sample events (containing at least one jet with a secondary vertex tag) is plotted versus the significance; we can observe that the cut $\mid L \mid / \sigma > 1$ allows to select events with more than 50% fraction of the signal, compared to the 30% of charm signal and to the 20% of light flavours.

3.5 Proper decay length

The distances L and L_{xy} defined in the above section, allow to evaluate the proper decay distance. If an unstable hadron with mean lifetime τ goes through the distance L before decaying, we have the relation:

$$L = c\beta t = c\beta\gamma t_p \tag{14}$$

where t is the time spent between the production and the decay of the hadron, $c\beta$ the hadron speed, $\gamma = (1-\beta^2)^{-2}$ and t_P is the proper time. If we indicate with M the mass of the hadron and with P and P_T its momentum

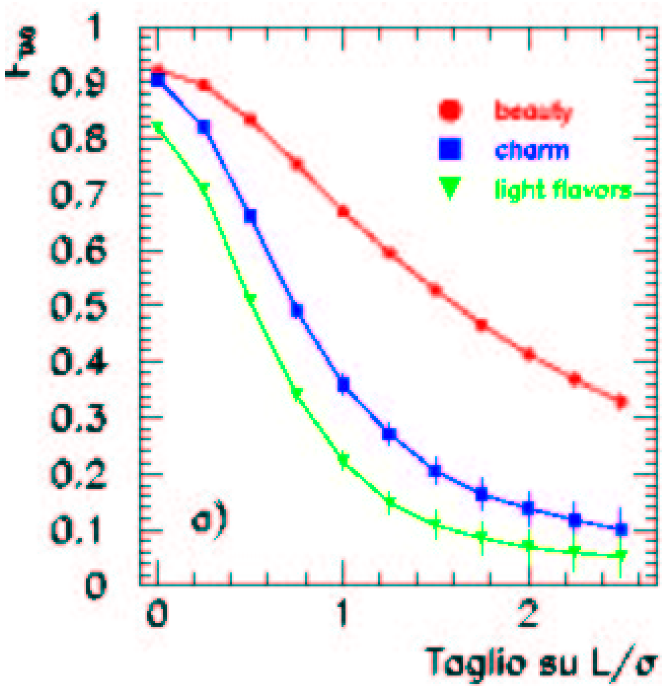

Figure 9: Fraction of events which survive to the different eta cuts.

and transverse momentum, from (14) we have:

$$ct_p \equiv c\tau = \frac{L}{\beta\gamma} = L\frac{M}{P} \tag{15}$$

or, in the transverse plane:

$$c\tau = L_{xy}\frac{M}{P_T}. \tag{16}$$

This variable turned (improperly) $c\tau$ correspond to the proper decay length. In an ideal situation this distribution is exponential, with a mean value equal to the $c\tau$ of the unstable hadron. Experimentally we should approximate M and P or P_T with quantity calculated with the available observables. We have two choices:

1. using the tracks associated to the considered secondary vertex

2. using reconstructed kinematic quantities of the jet which have a secondary vertex tag

In case 1., we estimate the mass, the momentum and the transverse momentum using tracking information; associating the mass of the pion m_π to each track considered:

$$P = \sum_i p_i \tag{17}$$

$$P_T = \sum_i p_{T,i} \tag{18}$$

$$M = \left[\left(\sum_i \sqrt{p_i^2 + m_\pi^2} \right)^2 - \left(\sum_i p_{xi} \right)^2 - \left(\sum_i p_{yi} \right)^2 - \left(\sum_i p_{zi} \right)^2 \right]^{1/2} \quad (19)$$

where the sums run over the number of tracks associated to the secondary vertex. In the second case instead we used the variables of jet with a secondary vertex tag. In the recombination scheme adopted in the k_T jet finding algorithm using massive jets we have:

$$P = P_{jet} = (P_{x,jet}^2 + P_{y,jet}^2 + P_{z,jet}^2)^{1/2} \quad (20)$$

$$P_T = P_{T,jet} = (P_{x,jet}^2 + P_{y,jet}^2)^{1/2} \quad (21)$$

$$M = (E_{jet}^2 - P_{jet}^2)^{1/2} \quad (22)$$

The formula above are only approximations of the true variable of the decaying hadron . In Fig. 10 are shown the corelation and the distribution of the ratios P/M and P_T/M, calculated using the jet variables with respect to those related to the heavy hadron correspondent to the jet.

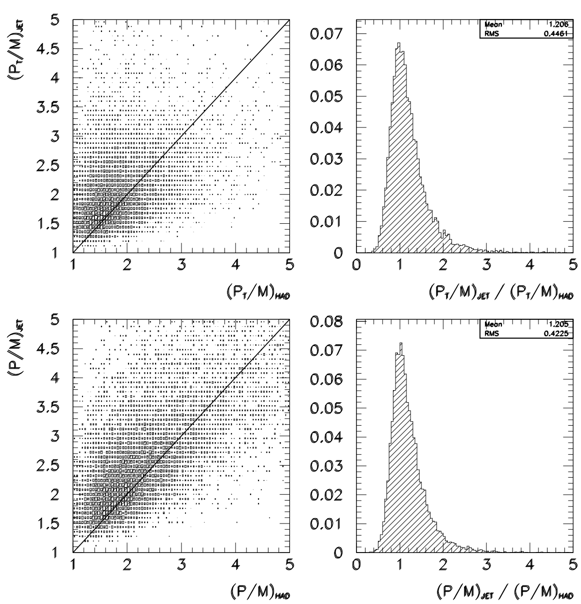

Figure 10: Correlation and distributions of the ratiosP/M and P_T/M calculated using the jet variables.

The figure 10 refers to the beauty sample in which the resolved and direct photoproduction component were combined normalizing them to the same luminosity. The same distributions are show in Fig. 11 using the tracking informations. We can observe a better correlation using the jet variables while there is a systematic underestimate of the mass w.r.t. the momentum when we use the tracking information.
For this reason we chose to use this jet quantities to estimate the kinematic factor which transform the decay

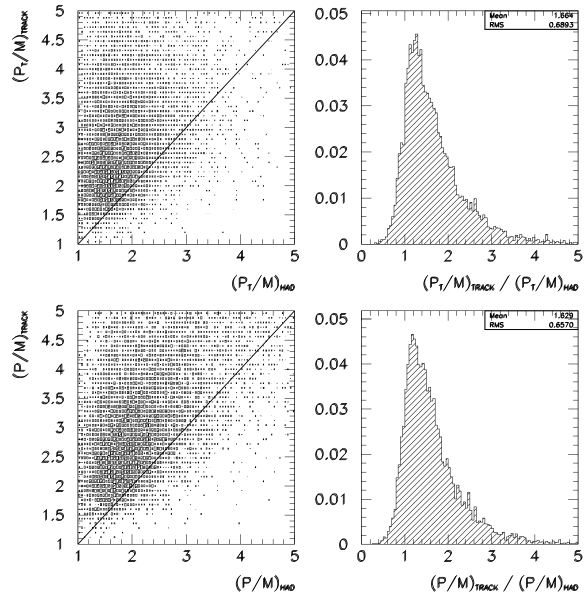

Figure 11: Correlation and distributions of the ratios P/M and P_T/M calculated using tracking information.

distance in the proper decay distance. In this preliminary study we did not consider the energy corrections for the jets which should take into account the energy losses of the particles crossing the inactive material before reaching the calorimeter.
The fig. 12 shows the proper decay distributions.

We can see that the background distribution (12 c)) is symmetric with respect to $c\tau = 0$ due to the finite MVD resolution, while the distribution related to the beauty signal (12 a))is quite asymmetric as we expected; for the charm signal we still observe an asymmetry even if it is less pronounced. Since the fraction of events in the signal sample (beauty) which present $L < 0$ is small it will be possible to estimate the background spectrum (light flavours) directly from the data, simmetrizing the negative part of L. In figure we required a significance cut $\mid L \mid /\sigma > 1$ which contributes to drop out the negative $c\tau$ area in the signal distribution of the heavy flavours. The $c\tau$ distribution of the heavy quark sample shows the characteristic exponential decay which is compatible with the mean lifetime of the hadrons containing beauty and charm.

4 Preliminary studies on 2002 data

During the shutdown period (2000-2001) HERA has been upgraded to reach higher luminosity. Due to high background conditions during the 2002 running no useful data for physics were taken.
In this section I will describe the application of some of

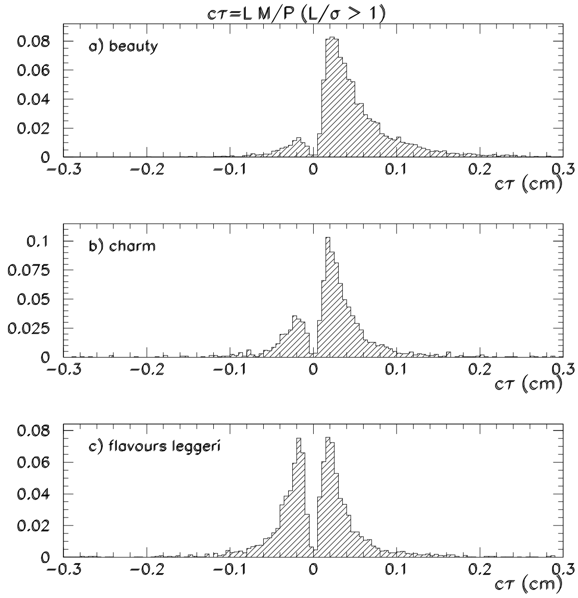

Figure 12: Proper decay distance distribution for a) beauty, b) charm and c)light flavours Monte Carlo samples.

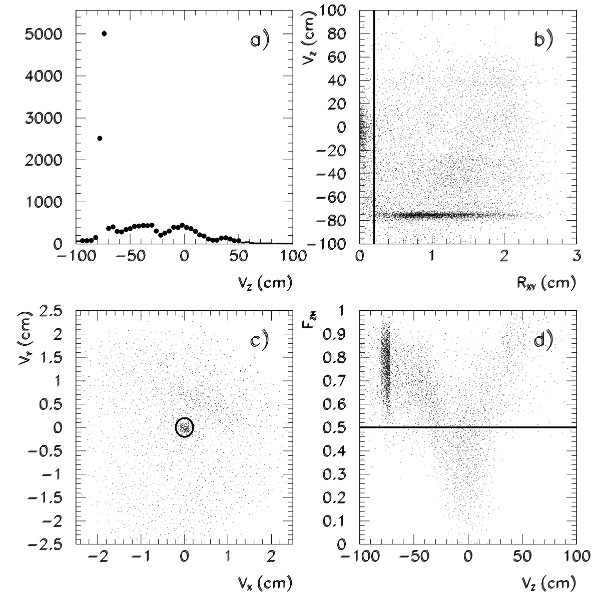

Figure 13: In a) V_z primary vertex coordinate distribution; in b)-c) the cut applied on R_{xy} and in d) theF_{z_H} cut.

the techniques developed with Monte Carlo to the real data, keeping in mind that the MVD-CTD system in that period was not yet aligned.

4.1 Event selection

The events were selected using a TLT filter for photoproduction events containing two jets with high transverse energy (the jets are determined at TLT with a cone algorithm). The selection criteria are:

- 2 jet, with $E_T > 8$ GeV, $\eta < 2.5$
- $P_Z/E < 1$
- $E - P_Z < 100$ GeV

The first and second level of trigger requirements are energy deposits over a certain threshold and activity in the tracking detector respectively. In fig. 13 we can see the primary vertex coordinate distribution V_z.

This distribution shows the presence of high background due to the interaction with the residual gas and with the material surrounding the beam-pipe. We can observe a peak in the distribution at $V_z = -80$ cm which corresponds to secondary interactions proton-beam gas upstream. In order to select events originating from the interaction point, we applied some "cleaning" cuts based on the tracking information. In fig. 13 b) is shown the correlation of the V_z w.r.t. the R_{xy} variable defined as:

$$R_{xy} = \sqrt{(V_x - \bar{V_x})^2 + (V_y - \bar{V_y})^2} \tag{23}$$

where the $\bar{V_x}$ and $\bar{V_y}$ are 1.81 cm and 0.19 cm respectively (values available from the recent data run). The event with a primary vertex inside the region around the effective interaction vertex are concentrated at small values of R_{xy} therefore we required $R_{xy} < 0.2$ cm in order to obtain a substantial background reduction. In fig. 13 c) we can see the correlation of the two coordinates V_x and V_y and again the applied cut which restricts the good zone where the possibly primary candidates can fall at a circumference of radius equal to 0.2 cm We can define the ratio F_{z_H} like:

$$F_{z_H} = \frac{N^{eliche}(z_H > 30cm)}{N^{eliche}_{tot}} \tag{24}$$

where at the numerator we have the number of tracks which have a Z_H coordinate of closest approach to the fit reference point ((x,y)=(0,0)) greater than 30 cm; the denominator represents the total number of helixes reconstructed in the event like showed in fig. 13 d) where the correlation between F_{z_H} and V_z is plotted; therefore we required an $F_{z_H} < 0.5$. Applying the above cuts on the V_z initial distribution the C5 peak disappeared and the background is significantly reduced (fig. 14).

The same event selection as described before for the Monte Carlo sample was applied:

1. at least two jets (k_T algorithm with "$E - recombination''$) with transverse momentum $P_{T1} >$ 8 GeV/c and $P_{T2} >$ 7 GeV/c and pseudorapidity $\mid \eta^{jet} \mid < 2.5$.
2. Rejection of events with a reconstructed electron in the final state with energy $E'_e > 5$ GeV and inelasticity $y_{el} \leq 0.9$

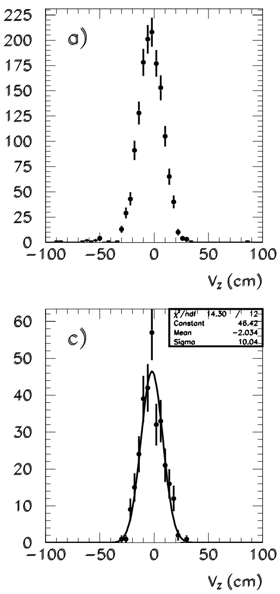

Figure 14: V_z primary vertex coordinate distribution a) after the geometrical cuts; in b) after the requirement of 2 jets with $P_{T1} > 8, 7$ GeV/c and $\mid \eta^{jet} \mid < 2.5$. In c) after the final selection $0.2 < y_{JB} < 0.8$ and after the rejection of electrons reconstructed in the final state.

3. $0.2 < y_{JB} < 0.8$

The distribution of the z coordinate V_z after requirement 1. and after all the requirements are shown in figure 14 d).

4.2 First comparison Data-Monte Carlo

In fig. 15 we compared light flavour Monte Carlo events ($\sim$ 25% direct and $\sim$ 75% resolved photoproduction) to the 2002 data. The number of Monte Carlo was normalized to the number of data. In fig. 15 we plotted the variables characterizing the two jets of the event with highest transverse momentum :$\eta^{jet}_{1,2}$, $P^{jet}_{T,1,2}$ and the invariant masses $M_{jet1,2}$. The η^{jet} distribution shows an excess of events in the forward region (positive η). The P_T distribution is quite well reproduced by the Monte Carlo. The invariant mass of the two jets of the event is peaked near 5 GeV and shows a good agreement between the data and the Monte Carlo.
Once we checked the good agreement between data and Monte Carlo regarding jets variables, we tried to see if this agreement was confirmed in the proper decay length distribution. In Fig. 16 the proper decay distance distributions are shown ($c\tau$ on top and $c\tau_{xy}$ at the bottom), comparing the simulated events with the data.
We can observe a good agreement between Monte Carlo and data. There are some disrepancies in the tails of the distributions (starting from $\mid c\tau \mid > 0.05$ cm) but this was expected since CTD and MVD was not alligned.

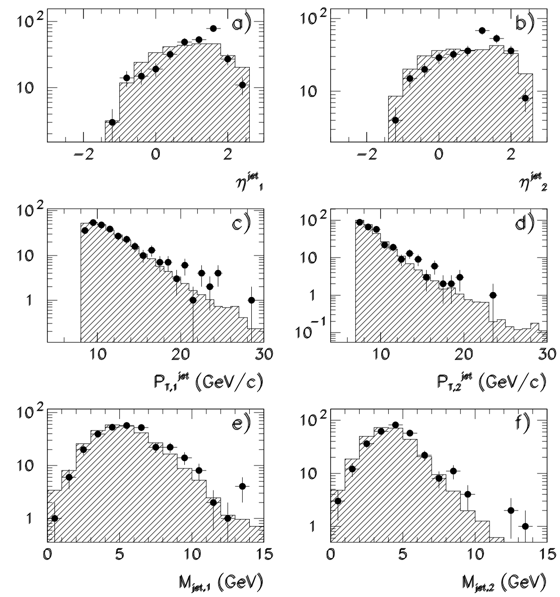

Figure 15: Comparison data-Monte Carlo for the jets variables.

To be noticed the very low statistics available (the number of events with at least a secondary vertex tagged which survived to the above mentioned cuts was equal to 116); the next step will be to include 2003 data in this distribution. At the moment I am also trying to use a procedure to re-fit the tracks which is based on the Kalman filter technique in which the multiple scattering and the other errors are more precisely evaluated.

5 Investigation of Forward Charm Production

The luminosity upgrade and the installation of the microvertex detector in ZEUS impose additional requirement on the pattern recognition and track reconstruction of the existing tracking detectors, particularly in the forward direction due to the HERA kinematics. The recent results from ZEUS on D^* photo-production [11] have shown an evidence for aboundant production in the forward region up to pseudorapidity of 1.5. Forward heavy flavour production in photoproduction and DIS interactions is of considerable interest because it can shed light on the parton content of the proton at high x and also it probes the intrinsic charm content of the photon.
The supplementation of the existing forward tracker with straw tube drift chambers covering the pseudo-rapidity range $1.5 < \eta < 3.0$ [12], will provide substantial improvement in efficiency and resolution of the forward tracking. Unfortunatelyy the STT information were not yet used in the tracking reconstruction (the software is still under development) but it will be very interesting to include them

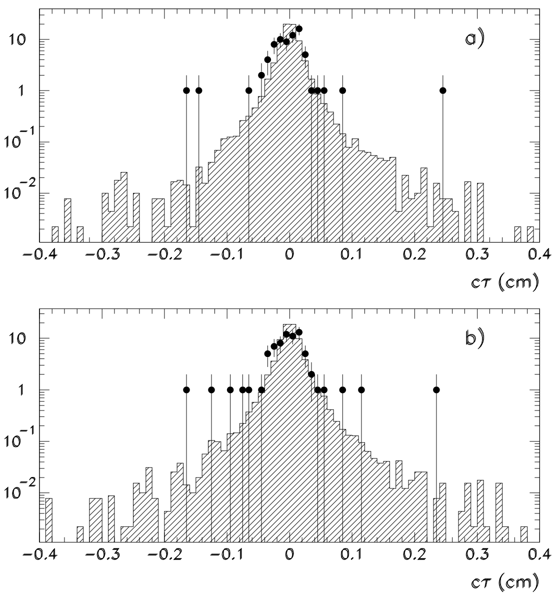

Figure 16: Comparison data-Monte Carlo for $c\tau$ (top) and $c\tau_{xy}$ (bottom) decay distance.

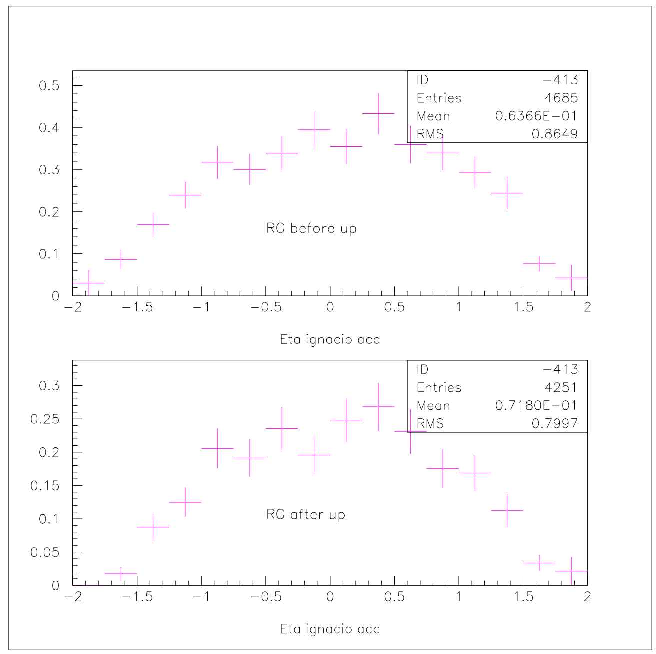

Figure 17: Distribution of the acceptance of D^* versus pseudorapidity η. On top Monte Carlo pre-upgrade are used, at the bottom post-upgrade configuration is taken into account.

in the analysis regarding the production of the charm in the forward region. For the time being we restrict the study of the D^* production to the pseudorapidity region $\eta < 2$. In Fig. 17 the distribution of the acceptance of the D^* versus η is plotted: in the top plot we used general D meson Monte Carlo events with the detector configuration before the upgrade made during the shutdown while at the bottom the simulated events are considering the new detector geometry. Only the CTD information were taken into account in this plot. The acceptance is significantly reduced in the second case, as expected, due to the presence of the MVD material inside the Central Tracking Detector. This is an important check because the existing measures of charm production do not extend at such forward region.
In fig. 18 the peak of the soft pion produced by the D^* decay is shown. Again we can observe at the top that the distribution obtained using Monte Carlo pre-upgrade is better than the bottom one which uses the post-upgrade configuration. We used the same 100000 generated events in both cases: in the first case we found 6051 D^* candidates, in the second one 609. We applied a cut on the D^* momentum $P_t > 1.5$ GeV/c and we consider the pseudorapidity $-2 < \eta_{D^*} < 2$ and $-2.0 < \eta_{track} < 2$.

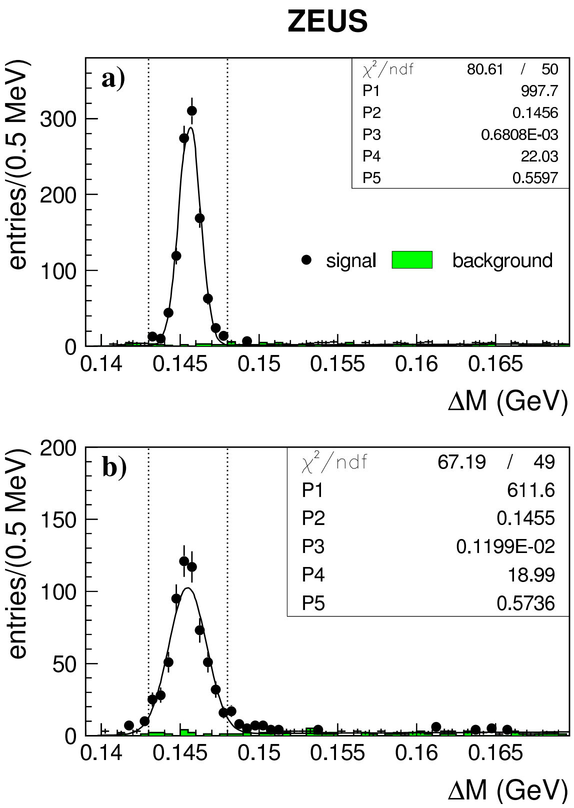

Figure 18: $\Delta M(D^* - D^0)$ distribution for a) pre-upgrade and b) post-upgrade configuration.

References

[1] HERA - A proposal for a alarge electron-proton colliding beam facility at DESY, report DESY HERA 81/10, July 1981.

[2] DESY PRC 97/01 A Micro Vertex Detector for ZEUS.

[3] DESY PRC 98/08 A Straw-Tube Tracker for ZEUS.

[4] G. Hartner, VCTRAK: Offline Output Information ZEUS-note 97-064.

[5] G. Hartner, VCTRAK Briefing: Program & Math ZEUS-note 98-058

[6] P. Billoir, S. Qian, Fast vertex fitting with a alocal parametrization of tracks, Nucl. Instr. and Meth., A234 (1985) 258.

[7] The ZEUS Detector Status Report 1993, DESY 1993.

[8] Geant 3.13 R. Brun, CERN DD/EE/84-1 (1987).

[9] S. D. Ellis and D. E. Soper, Phys. Rev. D 48 (1993) 3160.

[10] R. Sinkus, H. Abramovitz Electron Identification with Neutral Networks at ZEUS. ZEUS-note 93-117 08/11/93.

[11] ZEUS Collaboration, J. Breitweg et al., Phyis. Lett. B 401 (1997) 192.

[12] Capability of STT for Investigation of Forward Charm Production V.A. Bashkirov, D.Yu. Goloubkov ZEUS-note 98-066 September 24 1998